

PACS numbers: 42.65.Dr; 42.65.Es; 42.65.Hw
DOI: 10.1070/QE2011v041n11ABEH014697

Phasing of Stokes radiation under shock excitation of stimulated Brillouin scattering

A.A. Gordeev, V.F. Efimkov, I.G. Zubarev, S.I. Mikhailov

Abstract. **Interaction of counterpropagating waves in Brillouin-active media has been analysed by numerical computation. The dynamics of the development of acoustic waves is described using a second-order equation. It is shown that in the case of counterpropagating waves with sufficiently steep leading pulse edges ($\tau_f \leqslant 3T_2$, where T_2 is the acoustic phonon lifetime), SBS begins from the level of acoustic waves induced by shock excitation in the bulk of the active medium rather than from the spontaneous noise level. This mechanism determines the phase of the output Stokes wave, which is generated in the backward direction to the wave with the highest input intensity, irrespective of the ratio of counterpropagating-wave frequencies.**

Keywords: *phase conjugation, stimulated Brillouin scattering, absolute instability, shock excitation.*

1. Introduction

Numerous studies on the phase conjugation of laser radiation in the form of several beams, using stimulated Brillouin scattering (SBS) nonlinearity, showed that the necessary condition for implementing phasing of the output Stokes beams in different channels is the mutual interference of all input beams in the same volume of the active medium [1–3]. When four-wave mixing schemes are used to phase several channels, all input laser beams must interfere with the same reference wave [4, 5]. These requirements are quite obvious, because the aforementioned phase-conjugation systems implement not absolute but only relative phase conjugation of the beams interacting in the SBS mirror.

Recently, a new interferometric scheme (see Fig. 1a) has been proposed and implemented in a series of experimental studies [6–8]. Here, the initial laser beam is split into two beams by a semitransparent mirror, while the reflection from two independent SBS cells is obtained after transmitting the radiation through the active-medium volume, with subsequent backward focusing into the same volume. The experiments showed that the radiation reflected backward in the cells was frequency-shifted with respect to the incident radiation by the value of the Stokes shift, which is typical of the active medium used, while the phase difference of the two output waves barely changed in a series of independent experiments (Fig. 1b shows the phase difference realisations obtained in more than 200 independent tests [7]). The phase difference changed with a change in the position of the focusing mirrors M1 and M2 in the same way as in an interferometer with conventional mirrors. Hence, a direct conclusion is that the stimulated scattering starts developing not from the spontaneous-noise level. Meanwhile, we believe the theoretical interpretation of this effect that was proposed in [9] to be far from reality. The purpose of this study was to propose a correct interpretation.

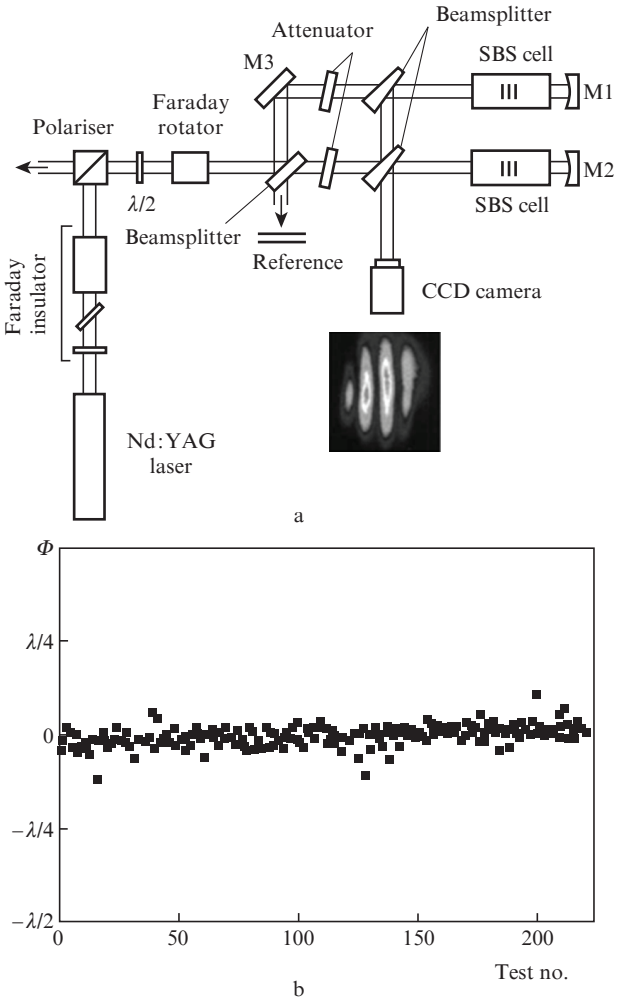

Figure 1. (a) Schematic of the experiment [7] and (b) the phase differences Φ of the output waves obtained in independent tests.

The effect under consideration can qualitatively be explained as follows: when two counterpropagating waves with the same

A.A. Gordeev, V.F. Efimkov, I.G. Zubarev, S.I. Mikhailov P.N. Lebedev Physics Institute, Russian Academy of Sciences, Leninsky prosp. 53, 119991 Moscow, Russia; e-mail: efimkov@sci.lebedev.ru, zubarev@sci.lebedev.ru, smekaelov@mailfrom.ru

Received 21 July 2011; revision received 12 October 2011
Kvantovaya Elektronika **41** (11) 997–1002 (2011)
Translated by Yu.P. Sin'kov

frequency are introduced into an active medium, a standing wave of density variation is generated in the bulk of the medium due to the occurrence of striction forces. If the leading edges of light pulses are sufficiently steep, shock excitation of intrinsic acoustic vibrations of the active medium occurs. Physical analogies of this process are the shock excitation of a resonant electrical circuit by a step voltage or vibrational excitation of a mechanical oscillator at a sharp transition to a new equilibrium state. Specifically these vibrations initiate stimulated scattering of input radiation. Therefore, in contrast to the concept proposed in [6–9], the generation of the intrinsic acoustic vibrations with frequencies in the vicinity of the SBS resonance is caused by not the standing grating of density variation but the high growth rate of this grating.

We analysed the interaction of counterpropagating waves in an SBS-active medium on the basis of numerical computation. To describe more adequately the dynamics of development of acoustic waves and their role in the process under consideration, we used the second-order equation for the first time. It is shown below that the time-dependent regime is characterised by generation of resonant acoustic waves under shock excitation of the active medium; the process studied occurs specifically on these waves under the conditions of absolute instability.

2. Basic equations and analysis

The analysis will be performed within the approximation of active medium with a length $L \ll \tau c$ (τ is the duration of interacting light pulses and c is the speed of light), which generally corresponds to the experimental conditions (the versions related to the compression of Stokes pulses due to the group-delay effects are disregarded). Then the time derivatives in the equations for the counterpropagating light fields can be neglected. Dynamics of the acoustic wave $Q(z,t) = q(z,t)\exp(\mathrm{i}k_q z)$ will be described by the second-order equation, which is exact for Raman scattering and approximate for Brillouin scattering. We assume that the interaction is local with respect to the active-medium response; therefore, we neglect the spatial derivatives in the equation for the amplitude $q(z,t)$; this approach is valid at short acoustic-phonon lifetimes T_2 and corresponds to the experimental conditions [6–8]. The counterpropagating waves can be considered as plane near the focal waist (where their interaction is most efficient) (see Fig. 1a). In this region, the wave propagating in the forward direction and the wave focused backward will be referred to as the signal and pump waves, respectively. Finally, the system of dynamic equations for the counterpropagating plane waves, according to the schematic diagram in Fig. 2a, can be written as

$$\begin{aligned}
&\frac{\partial a(z,t)}{\partial z} = 0.5 g_0 A(z,t) q^*(z,t),\\
&\frac{\partial A(z,t)}{\partial z} = 0.5 g_0 a(z,t) q(z,t),\\
&\frac{\partial^2 q(z,t)}{\partial t^2} + \frac{2}{T_2}\frac{\partial q(z,t)}{\partial t} + \omega_0^2 q(z,t)\\
&\quad = 2\mathrm{i}\frac{\omega_0}{T_2} A(z,t) a^*(z,t) + 2\mathrm{i}\frac{\omega_0}{T_2} F(z,t).
\end{aligned} \tag{1}$$

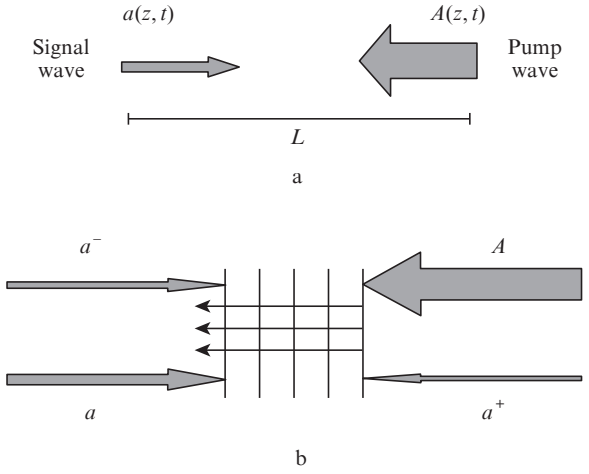

Figure 2. (a) Schematic diagram of interaction between the signal and pump waves and (b) the four-wave mechanism of generation of Stokes and anti-Stokes frequency components.

Here, z is the longitudinal coordinate (in the wave propagation direction); g_0 is the specific amplification increment of the Stokes signal upon SBS; $A(z,t)$ is the slow amplitude of the counterpropagating pump wave; $a(z,t)$ is the slow amplitude of the signal wave; $\omega_0 = |k_q v|$ is the Brillouin resonance frequency; v is the speed of sound in the active medium; T_2 is the acoustic-wave lifetime; $q(z,t)$ is the acoustic-oscillation amplitude, which is normalised so that the spatial derivatives of light-field amplitudes are proportional to g_0; and $F(z,t)$ is a δ-correlated thermal noise source of density fluctuations (it must be introduced to take into account the influence of spontaneous noise). Note also that, within these approximations, the wave vector of acoustic vibrations, k_q, is assumed to be $k_A + k_a$ (k_A and k_a are the moduli of the wave vectors of the pump and signal waves, respectively).

Obviously, system (1) remains valid when the counterpropagating waves have different frequencies. To explain the results of [6–8], the equality of the counterpropagating-wave frequencies will be specified.

To describe the process under consideration, system (1) was solved under the following boundary and initial conditions: $a(0,t) = a(t)\exp(\mathrm{i}\omega t)$, $A(L,t) = A(t)$, $q(z,0) = 0$, $q'(z,0) = 0$. Here, the pump-wave frequency is taken to be the origin of frequency coordinate and ω is the weak-wave frequency detuning from the counterpropagating-wave frequency.

The third equation for the acoustic vibrations of system (1) at step switching on light fields (with a noise source neglected and the light fields assumed to be specified with identical frequencies) yields the following estimate for the parameter $q(z,t)$:

$$\begin{aligned}
q(z,t) \sim\ & \frac{2\mathrm{i}}{\omega_0 T_2}\exp[\mathrm{i}(\varphi_A - \varphi_a)]\\
&\times\left\{1 - \exp\left(-\frac{t}{T_2}\right)\cos\left[\left(\omega_0^2 - \frac{1}{T_2}\right)^{1/2} t\right]\right\},
\end{aligned}$$

where φ_A and φ_a are the pump- and signal-wave phases. Having presented the cosine as half-sum of two exponentials and multiplied the expression for $q(z,t)$ by $\exp(\mathrm{i}k_q z)$, we obtain the solution for the acoustic waves in the form

$$Q(z,t) \sim \frac{\mathrm{i}}{\omega_0 T_2}\left\{2\exp(\mathrm{i}k_q z) - \exp\left[-\frac{t}{T_2} + \mathrm{i}(\omega_\mathrm{R} t + k_q z)\right]\right.$$

$$\left. - \exp\left[-\frac{t}{T_2} - \mathrm{i}(\omega_\mathrm{R} t - k_q z)\right]\right\},$$

Here, $\omega_\mathrm{R} = (\omega_0^2 - T_2^{-2})^{1/2}$ is the frequency of intrinsic acoustic vibrations of the medium. The first term describes the steady-state grating of the density of the medium, while the two others describe the acoustic waves propagating in the opposite directions. Specifically these waves initiate SBS of the input light fields. This fact was also experimentally confirmed in [10].

It follows from the above solution that the amplitude of shock-excited acoustic vibrations is inversely proportional to the product $\omega_0 T_2$. The active medium in [6–8] was Freon FC-75, which is characterised by the minimum product $\omega_0 T_2$ among the active media that are generally used in experiments; we believe this circumstance to be favourable for detecting the effect. The influence of a noise source in the equation for acoustic vibrations will be discussed below for specific time parameters of the pulses used in the experiments.

In the case of steady-state amplification of a small monochromatic signal, one can easily derive the well-known dependence of the gain on the signal frequency from system (1):

$$g(\omega) = g_0 f(\omega) = g_0 \frac{-2\mathrm{i}\omega_0 T_2^{-1}}{\omega_0^2 - \omega^2 + 2\mathrm{i}\omega T_2^{-1}}. \qquad (2)$$

Here, the pump-wave frequency, as was noted above, is taken to be the frequency coordinate origin.

The expression for $f(\omega)$ can be expanded in partial fractions:

$$f(\omega) = c\left(\frac{1}{1 + \mathrm{i}T_2(\omega_\mathrm{R} + \omega)} - \frac{1}{1 - \mathrm{i}T_2(\omega_\mathrm{R} - \omega)}\right), \qquad (3)$$

where $c = \omega_0/\omega_\mathrm{R}$. The first and second terms in (3) correspond to Stokes and anti-Stokes oscillation modes, respectively. Thus, one can clearly see that the frequency dependence of the gain is a superposition of two Lorentzian profiles, the first corresponding to the Stokes scattering and the second describing the anti-Stokes scattering. The corresponding dependences for Freon FC-75 and the pump wavelength λ = 1.064 μm are shown in Fig. 3 for the true profile $f(\omega)$ and its approximation by the Lorentzian profile $\varphi(\omega) = [1 + \mathrm{i}T_2(\omega_\mathrm{R} + \omega)]^{-1}$, which is generally used to describe SBS, with ω_R replaced by ω_0.

As was noted above, two counterpropagating light waves with equal frequencies and steep leading edges of pulses generate resonant acoustic waves in the active medium. As a result, the light waves undergo scattering from the moving density gratings to generate waves with Stokes and anti-Stokes frequency shifts with respect to the pump-wave frequency. In this case, the schematic diagram of interaction (Fig. 2b) corresponds to the four-wave mechanism. A specific feature of this scheme is the absence of spatial separation of the generated and pump waves. Note that Fig. 2b shows only one acoustic wave, which corresponds to the scattering of high-power pump with a Stokes shift. In this case, the second acoustic wave can be neglected in the qualitative analysis below, because its maximum intensity is much smaller; this is confirmed by the results of numerical simulation. At the ratio of counterpropagating-wave intensities $|A(z,t)|^2/|a(z,t)|^2 \sim 10$–$1000$ and sufficiently large gain increments ($\Gamma = g|A|^2 L \geqslant 4\pi$), the regime

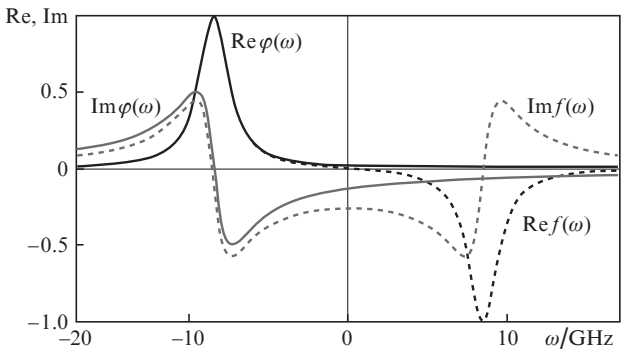

Figure 3. Dependences of the real and imaginary parts of the steady-state gain on the signal frequency: $\varphi(\omega)$ is the Lorentzian profile and $f(\omega)$ is the true profile given by (2). The coordinate origin corresponds to the pump frequency. The calculations were performed for Freon FC-75, proceeding from expressions (2) and (3).

of absolute instability for interacting waves is implemented [11, 12].

We will perform the analysis on the assumption that the amplitude of high-power pump wave ($A(z,t) = A = \mathrm{const}$) and the weak-wave intensity ($|a(z,t)|^2 = |a|^2 = \mathrm{const}$) are specified, taking into account the real gain profile (usually in the theoretical studies the pump-wave amplitude and the Lorentzian gain profile were considered to be specified *a priori*). On these assumptions, the steady-state equations for the amplitudes $a^-(z)$ and $a^+(z)$ of the Stokes and anti-Stokes waves, with the linear wave detuning neglected and the frequencies of the initial waves considered as equal, can be written as

$$\frac{\mathrm{d}a^-}{\mathrm{d}z} = \frac{g(\omega)}{2}(|A|^2 a^- + A a(z) a^{+*}),$$

$$\frac{\mathrm{d}a^{+*}}{\mathrm{d}z} = \frac{g(\omega)}{2}(A^* a(z)^* a^- + |a(z)|^2 a^{+*}), \qquad (4)$$

$$\frac{\mathrm{d}a(z)}{\mathrm{d}z} = -g_0 \frac{\mathrm{i}}{\omega_0 T_2}|A|^2 a(z).$$

Here, the phase modulation of a small-signal wave in the strong-wave field is taken into account in the third equation. One can easily solve the latter and, substituting the solution into the first two equations of system (4) and replacing the variables, reduce it to the system of two equations with constant coefficients. For brevity, we present the expression for the eigenvalues λ instead of the entire system, because, when the eigenvalues are known, one can find the conditions for existence of nonzero solutions under zero boundary conditions (specifically this is the criterion for implementing the absolute-instability mode):

$$\lambda^2 - \left[\frac{g(\omega)}{2}(|A|^2 + |a|^2) - \mathrm{i}\Delta\right]\lambda - \mathrm{i}\Delta\frac{g(\omega)}{2}|A|^2 = 0,$$

where $\Delta = g_0(\mathrm{i}/\omega_0 T_2)|A|^2$.

Having omitted some simple but cumbersome transformations, we present the final expression for determining the absolute-instability threshold:

$$\frac{\lambda_1 - \frac{1}{2}g(\omega)|A|^2}{\lambda_2 - \frac{1}{2}g(\omega)|A|^2} = \exp[(\lambda_2 - \lambda_1)L]. \qquad (5)$$

On the approximate assumption that

$$\lambda_1 \approx \frac{g(\omega)}{2}(|A|^2+|a|^2),\ \lambda_2 \approx -i\Delta \text{ и } \frac{|g(\omega)|}{2}|A|^2 \gg \Delta,$$

Eqn (5) for the generation frequencies ω and the minimum threshold gain increments $\Gamma_{th} = g_0|A|^2L$ yields

$$\ln\left(\frac{|A|^2}{|a|^2}\right) = \frac{\Gamma_{th}}{2}\mathrm{Re}(f(\omega)),$$
$$\Gamma_{th}\left[\frac{\mathrm{Im}(f(\omega))}{2} + \frac{1}{\omega_0 T_2}\right] = \pm\pi. \quad (6)$$

If the Lorentzian profile is used instead of $f(\omega)$ and the phase additive $(\omega_0 T_2)^{-1}$ in (6) is neglected, the solution to the system is the well-known result [11, 12], which leads to degeneracy in the threshold increment Γ_{th} due to the Lorentzian profile symmetry. In other words, the modes with equal frequency detunings from the gain-profile maximum have identical thresholds:

$$\Gamma_{th} = 2\left(\ln b + \frac{\pi^2}{\ln b}\right),$$
$$\omega = -\omega_R + \Omega, \quad (7)$$

where $\Omega = \pm\pi/(T_2 \ln b)$ and $b = |A|^2/|a|^2$.

This degeneracy causes strong output Stokes radiation oscillations at an appropriate frequency; these oscillations were observed in [13], where, due to the specificity of the active medium used (CS_2), the gain profile can be assumed to be Lorentzian and the phase additive can be neglected. The use of the real gain profile (2) in our case eliminates the degeneracy, and it can be shown that the mode with a frequency exceeding ω_R has a minimum threshold. Simultaneous consideration of the real profile and the nonlinear phase additive leads to the opposite result: the minimum threshold corresponds to the mode with a frequency lower than ω_R, because

$$\Omega \approx \frac{1}{T_2}\left(-\frac{\pi}{\ln b} + \frac{2}{\omega_0 T_2(1+\pi^2/\ln^2 b)}\right)$$

[this expression is obtained as a result of approximate solution of system (6)]. This leads to a decrease in the threshold increment in comparison with the value in (7). Anticipating things, we should note that the results of the numerical calculation confirm that the phase modulation of the weak pump wave must be taken into account (Fig. 5). Note also that, when counterpropagating pump waves with different frequencies are used, the sign of nonlinear additive will change (Fig. 3) and, correspondingly, the sign of Ω will also change to opposite (see Fig. 5).

3. Basic results

The computer simulation was performed using the Mathcad 14 Software. The numerical solution to system (1), which was obtained using the boundary and initial conditions, is a spatiotemporal matrix of amplitudes of the pump wave, the counterpropagating wave, and the acoustic wave; this form allows one to obtain the main wave characteristics (phase and intensity) in an arbitrary spatiotemporal cross section. The temporal profile of the pump pulses was chosen proceeding from the data of the above-mentioned studies. The ratio of the counterpropagating-wave intensities varied from 10 to 1000. A δ-correlated noise source $F(z,t)$ [see (1)] was simulated by the function $R\,\mathrm{rnd}(1)\exp[i\,\mathrm{rnd}(2\pi)]$.

Note also that system (1) is written for slow envelopes of the pulses propagating in opposite directions rather than for the amplitudes of spectral components at specified frequencies; i.e., there is a superposition of waves with different frequencies that are shown in Fig. 2b in each of the two directions. After the Fourier transform of the calculated pulses we can select the signal and pump waves and the Stokes and anti-Stokes components, because they have different carrier frequencies.

First, the calculations were performed for zero intensity of a small-signal wave at a steady-state gain increment $g_0 IL \sim 25$ (I is the pump-wave intensity) and a long (~50 ns) pump pulse with a smooth leading edge. In this case, the intensity of the output Stokes signal, which develops from the spontaneous-noise level, should be ~1% of the pump intensity; it is considered as the experimental SBS threshold. Based on specifically these considerations we found the noise source amplitude $R \sim 2\times10^4$ in system (1). Figure 4 shows the time dependences of the interacting-wave intensities at the maximum steady-state gain increment (35), the ratio of counterpropagating-wave intensities equal to 100, and equal frequencies of the signal and pump waves. Oscillations with a frequency close to the Stokes-shift frequency can clearly be seen in the output signal and in the output pump wave.

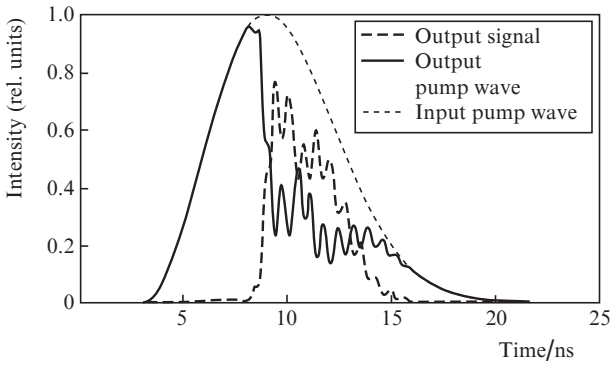

Figure 4. Time dependences of the interacting-wave intensities.

The spectral composition and phase behaviour of the interacting waves at different ratios of the pump and signal frequencies are shown in Fig. 5. The FWHM duration of the input pulses was assumed to be 7 ns. To model the real situation, the wave intensities during the first three nanoseconds were considered as zero in order to obtain the quasi-steady-state level of noise acoustic vibrations before switching on the interaction between the signal and pump waves. Qualitatively similar results were obtained at steady-state gain increments of 20–30. Figure 5 shows the cases where the input signal has resonant Stokes (Figs 5a, b) and anti-Stokes (Figs 5c, d) frequencies. Here, even in the case of anti-Stokes input signal, a Stokes-shifted wave (with respect to the pump wave) is recorded at the output (note that this holds true for only the interacting waves with the above-mentioned parameters). The spectra and phases in Figs 5e–h correspond to the cases where the input-signal frequency is within (Figs 5e, f) or beyond (Figs

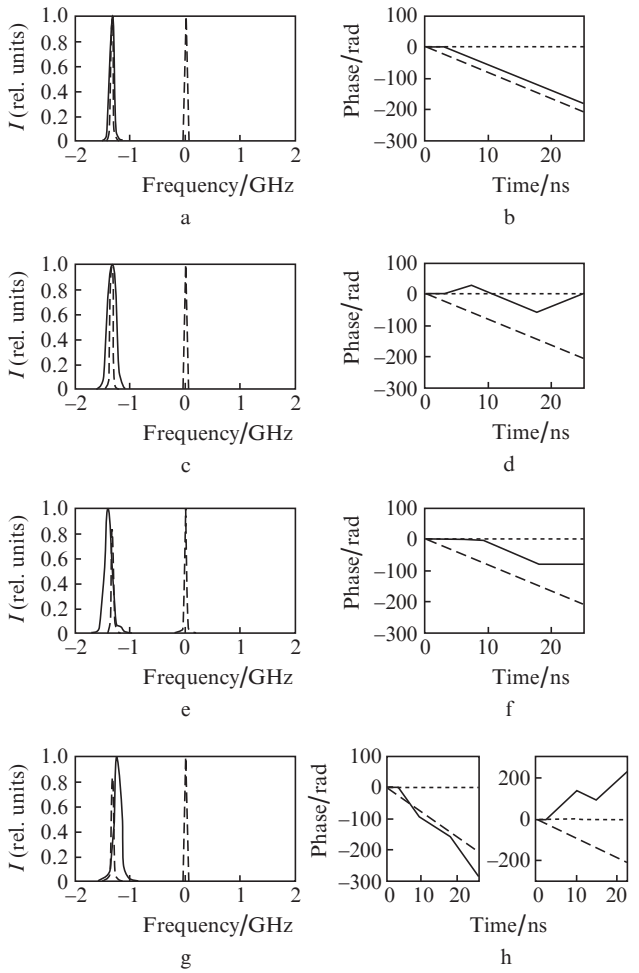

Figure 5. Spectra and phases of output waves for different input-wave frequencies: (a, c, e, g) the spectra of the output signal (solid lines) and the spectra of input pump wave and Stokes signal at the resonant frequency (dashed lines) and (b, d, f, h) the phases of the output signal (solid lines), the resonant Stokes signal (dashed lines), and the output pump wave (dotted lines). The cases (e, f) $\omega_s - \omega_p = 0$ and (g, h) $|\omega_s - \omega_p| > \omega_{res}$ are considered.

5g, h) the frequency band of the real SBS profile. One can see that the output-signal spectrum is shifted in a particular direction with respect to the exact resonance; this pattern is in complete agreement with the results of approximate analysis in Section 2.

The time dependences of output-wave phases are shown in Figs 5b, d, f, and h. As was noted above, the frequency coordinate origin is taken to be the pump-wave frequency. The phase of the resonant Stokes signal is shown as a reference in each panel. One can clearly see that in the beginning and in the end of interaction the output-signal phase is determined by the frequency of the weak input wave ω_s, and, when the Stokes-shifted (with respect to the strong wave) signal dominates in the output beam, the phase begins to be determined by the frequency corresponding to the Stokes shift ($\omega_s = \omega_p - \omega_R$) in the case of resonant excitation and the frequency with the corresponding detuning from the exact resonance at $\omega_s \neq \omega_p - \omega_R$. The time dependences of the output-radiation phase become almost parallel to the reference one. The transition to a particular type of temporal phase variation at a chosen time scale is almost stepwise due to the fast increase in the Stokes component of the output signal in the beginning of the pulse or its fast decrease in the end. It can also be seen that the pump-wave phase remains practically the same because at the chosen ratios of interacting-wave intensities it is still most intense along the entire interaction length.

Nevertheless, the presence of a wave withy a Stokes shift in the output signal does not mean stable reproducibility of the phase ratios of signals in a number of independent tests according to the technique [7].

If the term $F(z, t)$ in system (1) is neglected, the problem becomes completely deterministic, and the output-radiation phase (under zero initial conditions for acoustic vibrations) is determined by the input-signal phase. Indeed, the exact solutions to system (1) will differ by only the presence of the corresponding phase factors of the $\exp[i\varphi_{A,a}(0)]$ type for light fields and the $\exp[i\varphi_A(0) - i\varphi_a(0)]$ type for the acoustic wave, which can be proved by their substitution into system (1). The presence of a noise source should lead to the phase mismatch. Obviously, the average phase depends on the pump-wave intensity, the ratio of the pump- and signal-wave intensities, and the slope of the leading edge of interacting pulses. The most adequate characteristic is the rms deviation σ_N of the phase of the correlation coefficient $\mathrm{corr}[a(L, t), a(L, t)_n]$, since specifically this parameter determines the position of the interference patterns in the recording system (Fig. 1). Here, $a(L, t)$ and $a(L, t)_n$ correspond to the solutions to system (1) with the noise source neglected and taken into account, respectively; n is the test number; and N is the total number of independent tests. Figure 6 shows the dependence of σ_N on the width of the leading edges of the interacting pulses, which was determined from the time during which the pump intensity increased from $0.1I_{max}$ to $0.9I_{max}$. Each point in the plot corresponds to $N = 10$. The solid line $\sigma = \pi/\sqrt{3}$ shows the uniform phase distribution from 0 to 2π. All data were obtained at the ratio of pump and signal intensities equal to 100 and the maximum steady-state gain increment equal to 25. It can be seen that at the leading edge of the pulse duration up to $\sim 3T_2$ (in our case, $T_2 = 0.9$ ns), the phase reproducibility is sufficiently good; at the

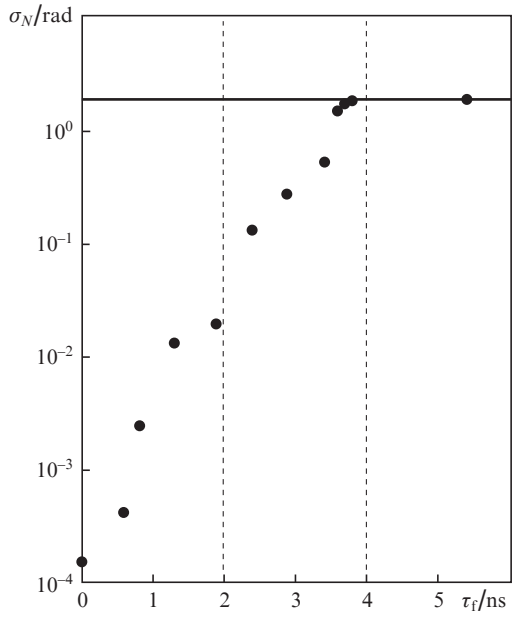

Figure 6. Dependence of the phase-reproducibility error in a number of independent tests on the durations of the leading edges of the pump and signal pulses at the input of the active medium.

pulse duration above $4T_2$ the phase distribution becomes independent of the initial signal phase and the output-signal phase starts being determined by a specific realisation of random spontaneous noise in each independent test.

4. Conclusions

We showed that the mode of shock excitation of acoustic vibrations can be implemented in the case of counterpropagating plane waves with steep leading edges ($\tau_f \leqslant 3T_2$). In this case the input-signal phase is reproduced in a number of independent tests. Note again that the main difference of the model of plane-wave interaction that was considered above from various versions based on the use of absolute instability on Brillouin nonlinearity is the absence of spatial separation of the signals with different frequencies. Therefore, by the analogy with the abbreviation BEFWM (Brillouin enhanced four-wave mixing), this scheme can be referred to asBEFWA (Brillouin enhanced four-wave amplification). Obviously, a conventional SBS amplifier is implemented when a signal is introduced at a Stokes shift frequency.

References

1. Basov N.G., Efimkov V.F., Zubarev I.G., Kotov A.V., Mikhailov S.I., Smirnov M.G. *Pis'ma Zh. Eksp. Teor. Fiz.*, **28** (4), 215 (1978).
2. Basov N.G., Efimkov V.F., Zubarev I.G., Kotov A.V., Mironov A.B., Mikhailov S.I., Smirnov M.G. *Kvantovaya Elektron.*, **6** (4), 765 (1979) [*Sov. J. Quantum Electron.*, **9** (4), 455 (1979)].
3. Basov N.G., Zubarev I.G., Mironov A.B., Mikhailov S.I., Okulov A.Yu. *Zh. Eksp. Teor. Fiz.*, **79**, 1678 (1980).
4. Basov N.G., Efimkov V.F., Zubarev I.G., Kotov A.V., Mikhailov S.I. *Kvantovaya Elektron.*, **8** (10), 2191 (1981) [*Sov. J. Quantum Electron.*, **11** (10), 1335 (1981)].
5. Pasmanik G.A., Khazanov E.A. *Kvantovaya Elektron.*, **16** (10) 2070 (1989) [*Sov. J. Quantum Electron.*, **19** (10), 1331 (1989)].
6. Kong Hong Jin, Lee Seong Ku, Lee Dong Won, Guo Hong. *Appl. Phys. Lett.*, **86**, 051111 (2005).
7. Lee S.K., Kong H.J., Nakatsuka M. *Appl. Phys. Lett.*, **87**, 161109 (2005).
8. Yoon Jin Woo, Shin Jae Sung, Beak Du Hyun, Kong Hong Jin. *Opt. Commun.*, **282**, 1000 (2009).
9. Kong Hong Jin, Lee Seong Ku, Yoon Jin Woo, Shin Jae Sung, Park Sangwoo. *Advances in Lasers and Electro Optics* (Croatia: INTECH, 2010).
10. Dement'ev A.S., Demin I., Murauskas E., Slavinskis N. *Kvantovaya Elektron.*, **41** (2), 153 (2011) [*Quantum Electron.*, **41** (2), 153 (2011)].
11. Bespalov V.I., Pasmanik G.A. *Nelineinaya optika i adaptivnye lazernye sistemy* (Nonlinear Optics and Adaptive Laser Systems) (Moscow: Nauka, 1988).
12. Zel'dovich B.Ya., Pilipetskii N.F., Shkunov V.V. *Obrashchenie volnovogo fronta* (Wave Front Conjugation) (Moscow: Nauka, 1985).
13. Anikeev I.Yu., Glazkov D.A., Zubarev I.G., Mikhailov S.I. *Kvantovaya Elektron.*, **18** (6), 718 (1991) [*Sov. J. Quantum Electron.*, **21** (6), 651 (1991)].